JCEC
THE JOURNAL OF ENGINEERING AND EXACT SCIENCES

OPEN ACCESS

The Journal of Engineering and Exact Sciences – jCEC, Vol. 08 N. 02 (2022)
journal homepage: https://periodicos.ufv.br/jcec
eISSN: 2527-1075
ISSN: 2446-9416

Computational investigation of thermal behaviors of the automotive radiator operated with water/anti-freezing agent nanofluid based coolant

Investigación computacional del comportamiento térmico del radiador automotriz operado con agua /agente anticongelante a base de nanofluidos refrigerante

Article Info:
Article history: Received 2022-01-12 / Accepted 2022-03-10 / Available online 2022-03-10
doi: 10.18540/jcecvl8iss2pp13977-01e

Ibrahim Ademola Fetuga
ORCID: https://orcid.org/0000-0002-1943-4234
University of Lagos, Nigeria
E-mail: fetugaebraheem@gmail.com
Olabode Thomas Olakoyejo
ORCID: https://orcid.org/0000-0001-9942-1339
University of Lagos, Nigeria
E-mail: oolakoyejo@unilag.edu.ng
Daniel Ejike Ewim
ORCID: https://orcid.org/0000-0002-7229-8980
Durban University of Technology, South Africa
E-mail: daniele@dut.ac.za
Joshua Kolawole Gbegudu
ORCID: https://orcid.org/0000-0003-2417-2520
University of Lagos, Nigeria
E-mail: jk.gbegudu@gmail.com
Adekunle Omolade Adelaja
ORCID: https://orcid.org/0000-0001-9175-8332
University of Lagos, Nigeria
E-mail: aadelaja@unilag.edu.ng
Olayinka Omowunmi Adewumi
ORCID: https://orcid.org/0000-0002-3545-6679
University of Lagos, Nigeria
E-mail: oadewunmi@unilag.edu.ng

Resumen
En este estudio, se llevó a cabo un estudio de dinámica de fluidos computacional (CFD) en 3D en ANSYS (FLUENT) para examinar el rendimiento térmico de un radiador de automóvil usando refrigerante convencional e híbrido con nanopartículas (NP) de Al_2O_3. Una mezcla híbrida de agua pura (H_2O) y etilenglicol (EG) en la proporción volumétrica de 50:50, se acopló con nanopartículas de Al_2O_3 con una fracción de volumen de 1% - 4% a diferentes temperaturas de entrada. El número de Reynolds se varió de 4 000 a 8 000. A partir de los resultados numéricos obtenidos, se encontró que un aumento en la fracción de volumen de nanopartículas condujo a un aumento en la tasa de transferencia de calor y una caída de presión en el radiador del automóvil. Además, se encontró que

a un número de Reynolds de 8 000, el uso de la mezcla híbrida como fluido base aumentó el número de Nusselt en un 55.6 % en contraste con el agua pura. Sin embargo, la suspensión adicional de nanopartículas de 4% Vol. Al_2O_3 en la mezcla híbrida existente aumentó el número de Nusselt en un 70%. Además, se encontró que un aumento en la temperatura de entrada del radiador provocó una mayor mejora en la tasa de transferencia de calor. Para Re=8 000, 4% Vol. Al_2O_3-nanofluido de agua, la tasa de transferencia de calor aumentó en un 54.57 % al aumentar la temperatura de entrada de 60ºC a 90ºC. Por lo tanto, se recomienda que los radiadores de los automóviles funcionen a una temperatura de entrada alta con nanofluido que contiene una concentración muy alta de nanopartículas adecuadas y un agente anticongelante en una proporción volumétrica adecuada para lograr un mejor rendimiento térmico.
Palabras-clave: Simulación. Nanofluido. Etilenglicol. Radiador automotriz. Mejora del calor.

Abstract
In this study, a 3D computational fluid dynamics (CFD) study was conducted in ANSYS (FLUENT) to examine the thermal performance of an automotive radiator using conventional and hybrid coolant with a Al_2O_3 nanoparticles (NPs) . A hybrid mixture of pure water H_2O and ethylene glycol (EG) in the volumetric proportion of 50: 50, was coupled with Al_2O_3 nanoparticles with volume fraction of 1% - 4% at different inlet temperatures. The Reynolds number was varied from 4 000 to 8 000. From the numerical results obtained, it was found that an increase in nanoparticle volume fraction led to an increase in heat transfer rate and pressure drop in the automotive radiator. Also, it was found that at a Reynolds number of 8 000, using the hybrid mixture as a base fluid increased the Nusselt number by 55.6% in contrast to pure water. However, further suspension of 4% Vol. Al_2O_3 nanoparticles into existing hybrid mixture increased the Nusselt number by 70%. Furthermore, it was found that an increase in the inlet temperature of the radiator caused more enhancement in the heat transfer rate. For Re=8 000 4% vol. Al_2O_3-water nanofluid, the heat transfer rate was enhanced by 54.57% when increasing the inlet temperature from 60ºC to 90ºC. Therefore, it is recommended that automobile radiators be operated at a high inlet temperature with nanofluid containing a very high concentration of suitable nanoparticles and an anti-freezing agent in an adequate volumetric proportion to achieve better thermal performance.
Keywords: Simulation. Nanofluid. Ethylene glycol. Automotive Radiator. Heat enhancement.

1. Introduction

The advancement of technology in the automobile industry has increased the demand for high performance engines, and to achieve this, carbon neutrality, fuel management, and reduction in weight of engine components (such as radiators and engine blocks) must be taken into consideration. To avoid derailing from the aim of this study, automobile radiators will be focused on. An automobile radiator is a heat exchange device that is incorporated into a vehicle to cool the large quantity of heat generated in the engine, thereby facilitating the efficiency and performance of the vehicle. If the engine is not properly cooled, setbacks such as deformation and failure of engine components and knocking may arise.

One of the many approaches to increasing the efficiency of radiators is by applying an anti-freezing agent to the base fluid, usually water, as a coolant to quickly transfer the heat generated in the engine (Ting et al., 2019). However, in some circumstances, the thermal performance of the coolant is usually called to question. For this reason, nanoparticles are now being used to increase the performance of coolants because of their high thermal conductivity (Abbasian Arani & Memarzadeh, 2021; Ebrazeh & Sheikholeslami, 2020; Zaharil, 2021).

Recently, several studies and efforts have been made by researchers to improve the cooling performance of radiator in vehicles of different kinds. (Peyghambarzadeh, Hashemabadi, Hoseini, et al., 2011; Peyghambarzadeh, Hashemabadi, Jamnani, et al., 2011) experimentally studied the

enhancement of heat transfer in a car radiator by using Al_2O_3/H_2O and Al_2O_3/EG nanofluid (NAF) as a coolant at varied flow rates (2-6 LPM) and fluid inlet temperature. They concluded that the Al_2O_3 NAF yields about 45% increase in the enhancement of heat transfer in contrast to pure water. (Oliet et al., 2007) explored a parametric study by investigating the factors influencing the performance of an automotive radiator.

The factors considered in this study include coolant and air mass flow rate, air temperature, and the density of the fin. They indicated that the performance of the radiator improves as the mass flow rate of air and coolant increase, at higher fin angles, smaller spacing between the fins, and lower air inlet temperature. (Trivedi & and, 2012) conducted a CFD analysis to investigate the effect of the varied pitch of tubes on automobile radiators. They suggested that a higher heat transfer rate can be achieved in radiators when the tube pitch is within the optimum value. The impact of dimples on forced convective heat transfer was analyzed by (Gadhave, 2012) and (Guntaka et al., 2009) examined. However, they found that the surface with dimples tends to have better heat transfer enhancement in contrast to the plain surface because of the turbulence caused by the dimples. (Nguyen et al., 2007), and (Chavan & Pise, 2013) used Al_2O_3/H_2O NAF to study thermal characteristics in a cooling system. At a volume fraction of 6.8% and 1% respectively. They both recorded about 40% increase in heat transfer coefficient at a volume fraction of 6.8% and 1% respectively. (Eastman et al., 2001) and (Heris et al., 2014) studied the effective thermal conductivities of EG having 0.3%, and 2.5% copper nanoparticle concentration respectively. They concluded that heat transfer is enhanced by approximately 40% and 50% respectively, compared to EG without a nanoparticle. (Nabil et al., 2020) experimentally investigated heat rejection and exit temperature of the Cu and CuO-H_2O based NFs in the vehicle radiator with concentration ranging from 1% to 4%. They indicated that Cu with 2% nano concentration has the maximum heat rejection rate and the lowest temperature at the exit of the radiator. (Habeeb et al., 2020) numerically explored the performance of spark ICE radiators consisting of fins made of Al, Cu, and Br with EG-based nanofluid of volume fraction ranging from 20% to 60%. They claimed that fins made of Cu offered the best performance in lowering the temperature of the ICE. (Umirov & Abdurokhmonov, 2021) developed an algorithm for estimating the finned plate water radiator. They proposed that their algorithm is efficient enough in selecting the most suitable design parameters for the radiator.

From previous studies, it is evident that either H_2O or EG is used as a base fluid in automotive radiators. Therefore, this study is unique in that it assesses the heat transfer charateristics of Al_2O_3 hybrid-based fluid (i.e., a mixture of H_2O and EG is used as base fluid) and Al_2O_3/H_2O NAF in an automotive radiator at different nanoparticle concentrations.

2. Methodology

2.1 Model Description

The ANSYS design modeler was used to create the geometry of the automotive radiator used in this study. The radiator contains three main parts, which are the inlet, flat tubes and fins (body), and outlet. The schematic diagram of the geometry configuration in several views is shown in Fig. 1(a)-(d). The information on the dimensions of the proposed automotive radiator is given in Table 1.

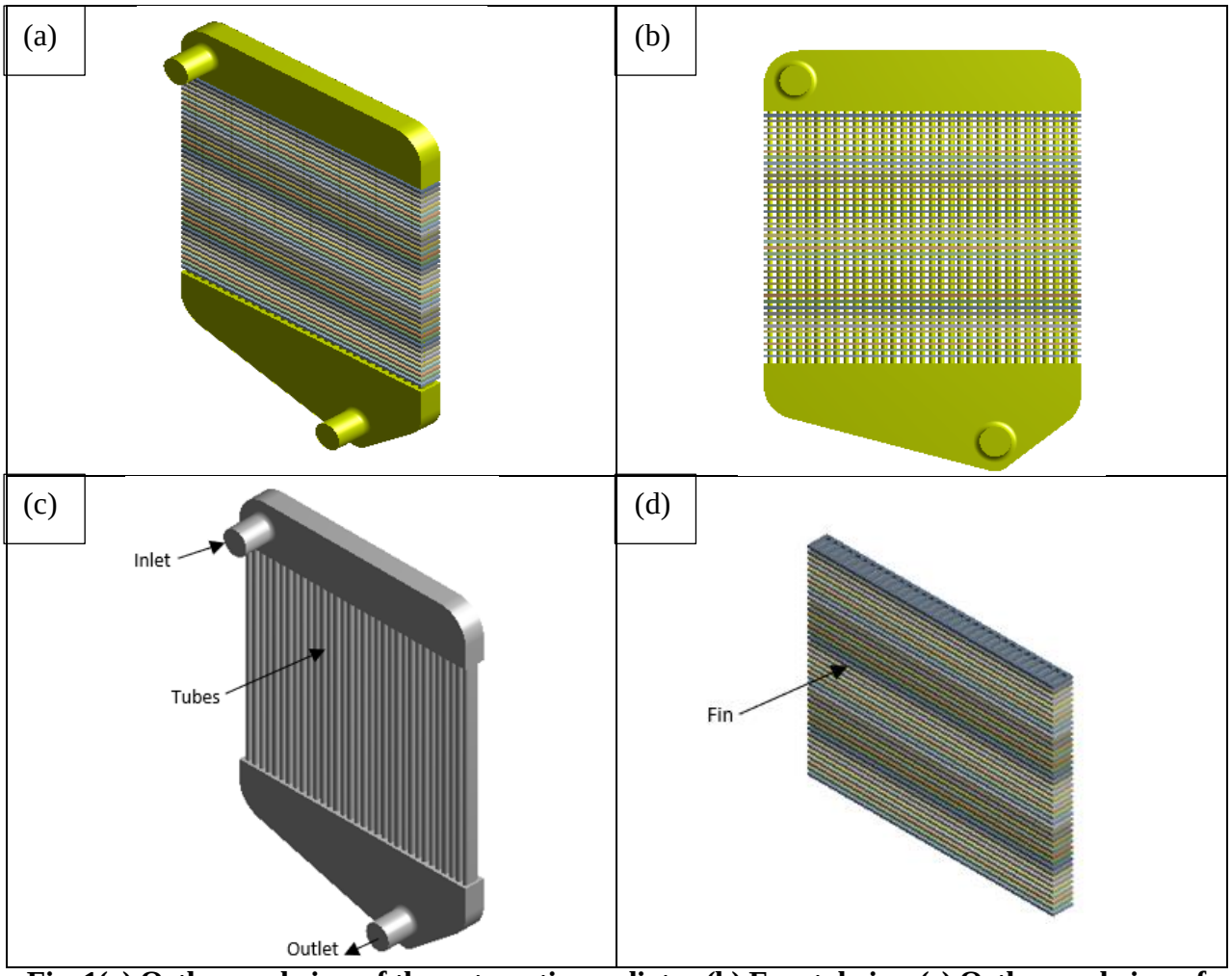

Fig. 1(a) Orthogonal view of the automotive radiator (b) Frontal view (c) Orthogonal view of the tube side (d) orthogonal view of the fin side

Table 1: Dimension and specification details of geometry configuration

Description	Unit/Specification
Inlet/outlet pipe diameter	50 mm
Radiator height	700 mm
Radiator length	500 mm
Radiator width	40 mm
Tube height	420 mm
Tube length	10 mm
Tube width	30 mm
Number of tubes	33
Tube spacing	7.5 mm
Tube arrangement	Linear
Fin thickness	5 mm
Fin width	40 mm
Fin spacing	5 mm
Number of fins	41
Material used	Aluminum

2.2 Mesh Generation

Effective numerical discretization is important to maximize the computational resources and to achieve accurate results. As shown in Fig. 2(a) through 2(b), ANSYS mesh was used to generate an

unstructured patch conforming tetrahedron mesh for all the domains of the proposed geometry, with an element size of 5mm assigned to the body of the radiator and 0.1 mm to the fin side. As shown in Table 2, It has been found that mesh quality measures such as skewness, orthogonality quality, and aspect ratio are all within the acceptable range.

Table 2: Mesh quality report

Quality	Maximum Value	Acceptable Range
Orthogonality Quality	0.8569	> 0.75
Aspect Ratio	35.614	< 100
Skewness	0.6032	< 0.85

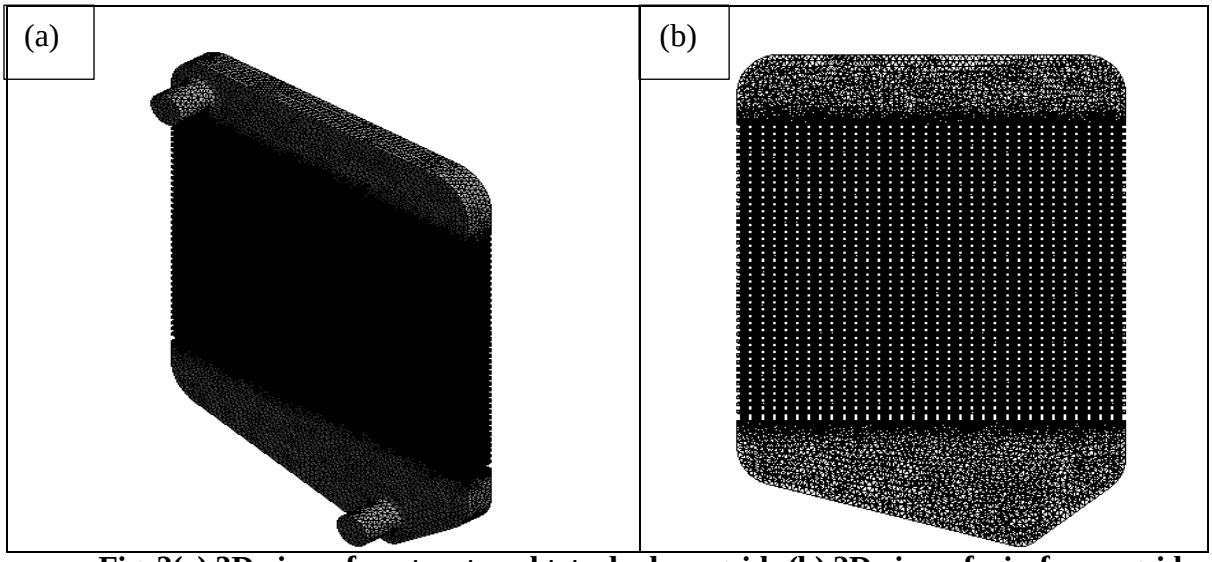

Fig. 2(a) 3D view of unstructured tetrahedron grids (b) 2D view of wireframe grid

2.3 Problem Formulation

This subsection summarizes the governing equations, assumptions, and boundary conditions (see Table 4) employed to solve the proposed study. The flow and heat transfer problems in the automotive radiator were solved by using the 3D incompressible steady Navier-Stokes equation. The RNG (k-ε) k-epsilon equation was used because of the possible laminar-transition-turbulence flow in the radiator. The governing equations are further simplified for the ease of solving the flow and heat problems based on the following assumptions (Manca et al., 2012):

1. Steady-state, turbulent, single phase, 3D incompressible nanofluid flow and heat transfer
2. Thermo-physical properties of the fluid and solid are constant
3. Thermal radiation, natural convection, gravitational and magnetic force are ignored
4. Viscous dissipation is neglected.

The governing equations are as follows:

Continuity Equation

$$\frac{\partial}{\partial X_i}(\rho X_i) = 0 \tag{1}$$

Momentum Equation

$$\frac{\partial(\rho U_i U_j)}{\partial X_j} = \frac{\partial P}{\partial X_i} + \frac{\partial}{\partial X_j}\left[\mu\left(\frac{\partial U_i}{\partial X_j} + \frac{\partial U_j}{\partial X_i} - \frac{2}{3}\delta_{ij}\frac{\partial U_k}{\partial X_k}\right)\right] + \frac{\partial}{\partial X_j}\left(-\rho\overline{U_i' U_j'}\right) \tag{2}$$

Where Reynolds stresses is indicated by $-\rho\overline{U_i' U_j'}$

$$-\rho\overline{U_i' U_j'} = U_i\left(\frac{\partial U_i}{\partial X_j} + \frac{\partial U_j}{\partial X_i}\right) - \frac{2}{3}\left(\rho k + U_t\frac{\partial U_k}{\partial X_k}\right)\partial_{ij} \quad (3)$$

Energy Equation

$$\frac{\partial(\rho U_i U_j)}{\partial X_j} = \frac{\partial P}{\partial X_i} + \frac{\partial}{\partial X_j}\left[\mu\left(\frac{\partial U_i}{\partial X_j} + \frac{\partial U_j}{\partial X_i} - \frac{2}{3}\delta_{ij}\frac{\partial U_k}{\partial X_k}\right)\right] + \frac{\partial}{\partial X_j}\left(-\rho\overline{U_i' U_j'}\right) \quad (4)$$

$$E = h - \frac{P}{\rho} + \frac{u^2}{2} \quad (5)$$

where turbulent viscosity (μ_t) is expressed as;

$$u_t = \frac{\rho C_\mu k^2}{\varepsilon} \quad (6)$$

Therefore, turbulent kinetic energy (k) is defined as

$$\frac{\partial}{\partial X_i}(\rho k U_i) = \frac{\partial}{\partial X_j}\left[\left(\mu + \frac{\mu_t}{\sigma^k}\right)\frac{\partial k}{\partial X_j}\right] + G_k - \rho\varepsilon \quad (7)$$

ε is dissipation rate, and is expressed as;

$$\frac{\partial}{\partial X_i}(\rho\varepsilon U_i) = \frac{\partial}{\partial X_j}\left[\left(\mu + \frac{\mu_t}{\sigma^\varepsilon}\right)\frac{\partial \varepsilon}{\partial X_j}\right] + C_{1\varepsilon}\frac{\varepsilon}{k}G_k - C_{2\varepsilon}\rho\frac{\varepsilon^2}{k} \quad (8)$$

Where destruction rate $(\rho\varepsilon)$ and generation rate (G_k) can be defined as;

$$G_k = -\rho\overline{U_i' U_j'}\frac{\partial U_j}{\partial X_i} \quad (9)$$

The constants used for turbulent transport equations are; $C_\mu = 0.09$, $C_{1\varepsilon} = 1.44$, $C_{2\varepsilon} = 1.92$, $\sigma_k = 1$, $\sigma_\varepsilon = 1.3$

Nanofluid thermophysical properties

Al_2O_3/H_2O EG-based NAF are used, considering the volume fraction($\emptyset$) of Al_2O_3 nanoparticles (NPs), which varied from 1% to 4%. The material properties of water, EG and Al_2O_3 NPs employed for the studies are presented in Table 2 below. The following are the effective properties of the NAF:

Density correlation (Fedele et al., 2012)

$$\rho_{NAF=}(1-\emptyset)\rho_F + \emptyset\rho_{NP} \quad (10)$$

Specific heat correlation (Ho et al., 2008)

$$\rho_{NAF}Cp_{NAF} = (1-\emptyset)Cp_F + \emptyset Cp_{NP} \quad (11)$$

Dynamic viscosity (Masoumi et al., 2009)

$$\mu_{NAF} = \mu_F + (\rho_{NP}U_B d_{NP}^2/72C\delta) \quad (12)$$

Where δ is the boundary layer thickness and U_B is Brownian velocity, both could be expressed below as:

$$U_B = \frac{1}{d_{NP}}\sqrt{\frac{18K_BT}{\pi\rho_{NP}d_{NP}}}, \text{and } \delta = \sqrt[3]{\frac{\pi}{6\emptyset}}d_{NP} \quad (13)$$

Where d_{NP} and K_B represent NP diameter and Boltzmann constant

$$C = \mu_{NAF}{}^{-1}[(z_1 d_{NP} + z_2)\emptyset + (z_3 d_{NP} + z_4)] \quad (14)$$

Where mean diameter of NPs and is expressed in nanometer.

$$z_1 = -0.000001133, z_2 = -0.000002771$$
$$z_3 = 0.00000009, z_4 = -0.000000393 \quad (15)$$

Thermal conductivity (Chon et al., 2005)

$$k_{NAF} = k_F \left[164\emptyset^{0.746} \left(\frac{d_F}{d_{NP}}\right)^{0.369} \left(\frac{k_{NP}}{k_F}\right)^{0.746} (Pr_{NAF})^{0.9955} (Re_{NAF})^{1.2321}\right] \quad (16)$$

Where Pr_{NAF}, Re_{NAF}, and K_B are expressed as:

$$Pr_{NAF} = \frac{\mu_{NAF}}{\rho_{NAF}\alpha_{NAF}} \quad (17)$$

$$Re_{NAF} = \frac{\rho_{NAF}\, k_B T}{3\pi\mu_{NAF}^2 l_{mf}} \quad (18)$$

$$K_B = 1.3807e^{-23} \quad (19)$$

Where l_{mf} represents the mean-free path of the base fluid.

Heat transfer coefficient calculations

The following procedures were taken with respect to Newton's cooling law to obtain the rate at which heat is transferred (Incropera et al., 1996):

$$Q = h_{expt} A_s \Delta T = h A_s (T_b - T_w) \quad (20)$$

$$T_b = \frac{T_i - T_o}{2} \quad (21)$$

The rate of heat transfer (Q) can also be written as follows:

$$Q = \dot{m} C_p \Delta T = \dot{m} C_p (T_i - T_o) \quad (22)$$

$$\dot{m} = \rho \dot{V} = \rho U A_t \quad (23)$$

Eq. (20) is substituted in Eq. (21) to obtain the heat transfer coefficient in Eq. (24)

$$h_{expt} = \frac{\dot{m} C_p (T_i - T_o)}{A_s (T_b - T_w)} \quad (24)$$

Thus, Nusselt number (Li et al., 2014) can be obtained as follows:

$$Nu = \frac{h_{expt}\, D_H}{k} \quad (25)$$

Reynolds number (Belnap et al., 2002) is calculated as;

$$Re = \frac{\rho U D_H}{\mu} \quad (26)$$

Friction factor (Saysroy & Eiamsa-ard, 2017) can be defined as;

$$f = \frac{2\Delta P}{\frac{L}{D_H}\rho U^2} \quad (27)$$

Where A_s represents the surface area of the tubes, $\dot{m}$ indicates mass flow rate, T_b denotes the bulk temperature, T_w represents the tube wall temperature, T_i denotes the inlet fluid temperature, T_o indicates the fluid outlet temperature, and C_p signifies the fluid specific heat capacity. A_t indicates the tube cross-sectional area, D_H represents the tube hydraulic diameter, L represents tube length, ρ denotes fluid density, f represents fanning friction factor, $\dot{m}$ indicates mass flow rate, ΔP indicates pressure drop and mean inlet velocity is represented by U.

Table 3. Material properties (Roy et al., 2004) **for base fluid and nanoparticles at 300K**

Material	$\rho(kgm^{-3})$	$C_p(Jkg^{-1}K^{-1})$	$k(Wm^{-1}k^{-1})$	$\mu(Pa.s$
Pure water	998.2	4 182	0.6	0.001003
EG	1 114.4	2 415	0.252	0.0157
Al_2O_3	3 970	765	40	-

Table 4. Boundary condition

Inlet velocity	Corresponding Reynolds number (4 000-8 000)
Coolant inlet temperature (T_i)	90 ^{0}C-60 ^{0}C
Pressure outlet	0 Pa
Wall of the tubes (convection boundary condition)	10 W/m^{2}k
Air temperature (T_a)	35 ^{0}C

3. Numerical Procedures

The ANSYS (FLUENT) commercial code was used as a simulation tool to solve the problem, $k-\varepsilon$ turbulent model with options of standard, realization, and enhanced wall treatment was adopted to perform the analysis under the finite volume approach of a SIMPLE algorithm. The least-square cell based was set for the spatial discretization scheme, second-order was set for pressure, the second-order upwind scheme was set for both momentum and energy equations, and turbulent kinetic energy and turbulent dissipation rate were both solved with the second-order upwind scheme. The default value was used for under-relaxation factors, and convergence criteria of 1e-6 were set for all the equations.

4. Results and Discussions

4.1 Grid independence Test

To select a suitable grid for this study, a grid sensitivity test was implemented in ANSYS (FLUENT) software for six different cases of grids based on the coolant outlet temperature of the radiator to reduce computational time. As shown in Table 5, the coolant outlet temperature of Al_2O_3/H_2O NAF with a nanoparticle concentration of 1% and a mean diameter of 25 nm for Reynolds number 8 000 was compared for different grids stated above. It was observed that by further increasing the grid size beyond **case 5** shows no significant change in coolant outlet temperature. Therefore, **case 5** was selected for this computational study.

Table 5. Grid independence data coolant outlet temperature for Al_2O_3-water nanofluid at Re = 8 000, $\emptyset = 1\%$

Mesh	Node	Element	T_{out} (^{0}C)
Case 1	709081	1109286	79.3
Case 2	757716	1648542	80.4
Case 3	801975	2368651	83.1
Case 4	819618	3143221	86.6
Case 5	929422	3870183	88.2
Case 6	980089	5268302	88.4

4.2 Validation of Model

The model is validated by contrasting the simulated results of Al_2O_3 − water NAF entering the radiator at an inlet temperature of 90 ^oC and a volume fraction of 4% for 4 000 ≤ Re ≤ 8 000 with the empirical correlation of Dittus- Boelter and Pak and Cho. As presented in Fig. 4, a good agreement is established between the numerical data and the available correlations. The maximum relative error between the simulated result and the Dittus-Boelter correlation is 3.66%, while the value is -1.75% in the Pak and Cho correlation. This led to providing confidence in the accuracy of our proposed model.

Dittus-Boelter correlation (F.W. Dittus & L.M.K. Boelter, 1930)

$$Nu = 0.023Re^{0.8}Pr^{0.3} \quad (28)$$

Pak and Cho correlation (Pak & Cho, 2007)

$$Nu = 0.021Re^{0.8}Pr^{0.5} \quad (29)$$

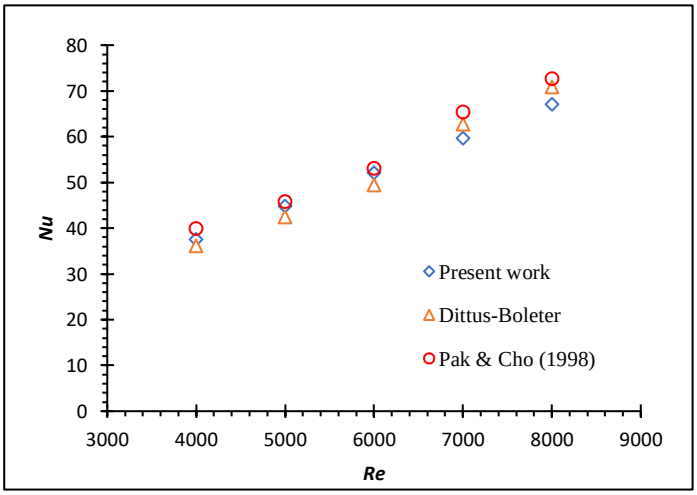

Fig. 4. Comparison of simulated results for Al_2O_3/water NAF with avaialble correlations.

4.3 Influence of volume fraction of aluminum nanoparticles on thermal performance

Fig. 5, 6, 7, and 8 show the effect of volume fraction of Al_2O_3 NPs with a mean diameter of 25 nm at an inlet temperature of 90 ^oC for different Reynolds number (*Re*) ranging from 4 000 to 8 000 on the Nusselt number (*Nu*), heat transfer rate, pressure drop (ΔP), and skin friction factor(f), respectively. As shown in Fig. 5, the *Nu* number uniformly increases with the Re in all cases of the volume fraction. It is revealed that the Nu becomes more intense as the volume fraction of NPs increases from 0% to 4%. At *Re*=8 000, 1.55 times the *Nu* of pure water is obtained by adding 4% of Al_2O_3 NPs, whereas 3%, 2%, and 1% of NPs yield 1.42, 1.29, and 1.14 times the Nu of pure-water, respectively. It is indicated in Fig. 6 that the heat transfer rate increases with the Re and volume fraction of the Al_2O_3 NPs. At 4 000 ≤ Re ≤ 8 000, 4% vol has the highest rate of heat transfer while, pure

water has the lowest heat transfer rate. Meanwhile, at Re=8 000, suspending a 4% volume fraction of NPs into pure water enhanced the cooling rate of the radiator by 2.29%. However, using 3%, 2%, and 1% vol increases the rate of heat transfer by 1.97%, 1.58%, and 0.97% as followed. The reason for this is that when NPs are suspended to the base fluid, random motion is generated to reduce the thermal boundary layer, which in turn increases the heat transfer enhancement. As illustrated in Fig. 7, the ΔP (pressure drop between the inlet and outlet of the automotive radiator) increases with Re as $\emptyset$ of nanoparticles rises. At $Re = 8\,000$, pressure drop of $13.9239\ Pa$, $8.62749\ Pa$, $5.02203\ Pa$, and $2.70952\ Pa$ are achieved by adding 4%, 3%, 2%, and 1% Al_2O_3 NPs, respectively, in contrast to a pressure drop of 1.33869 Pa for pure water. Subsequently, at Re = 4 000, pressure drop of 3.3909 Pa, 2.10108 Pa, 1.22279 Pa, and 0.659974 Pa are obtained by suspending 4%, 3%, 2% and 1% Al_2O_3 NPs into pure water. In Fig. 8, the results reveal that for all cases of volume fraction, the f decreases as the Re rises from 4 000 to 8 000. At $4\,000 \leq Re \leq 8\,000$, no significant change in f is reported as $\emptyset$ increases from 1% to 4% or vice versa.

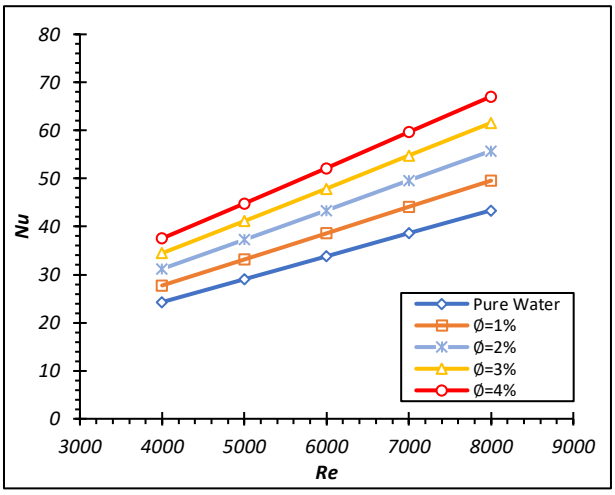

Fig. 5. Nu of Al_2O_3 − water NAF vs Re for different $\emptyset$ at $T_i = 90\ ^oC$

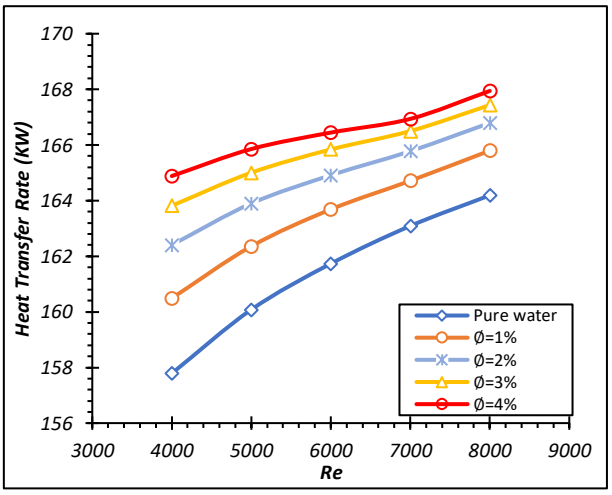

Fig. 6. Heat transfer rate of Al_2O_3 − water NAF vs Re for different volume fractions ($\emptyset$) at $T_i = 90\ ^oC$

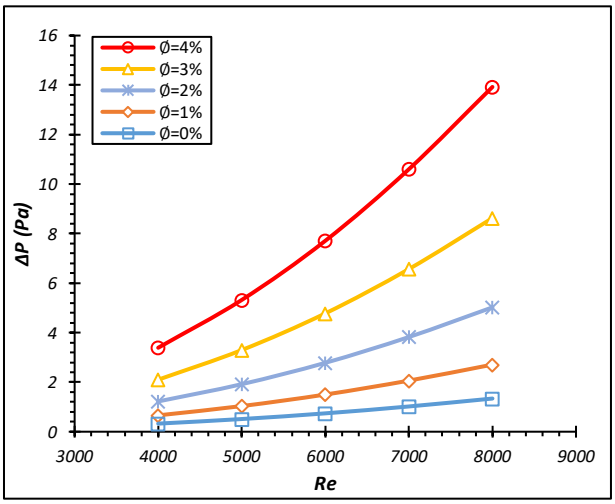

Fig. 7. Pressure drop of Al_2O_3-H_2O NAF vs Re for different volume fractions at $T_i = 90^oC$

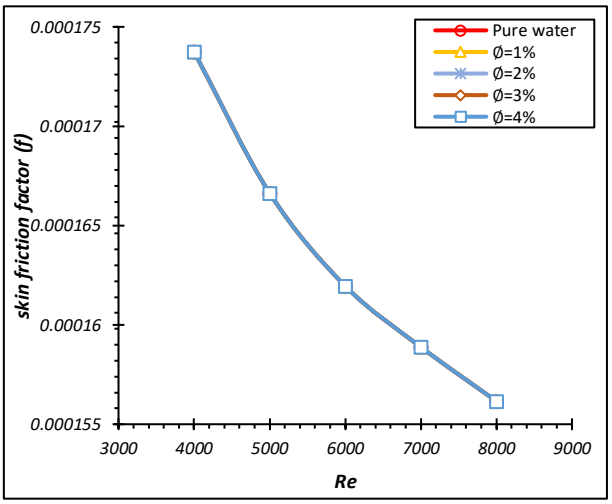

Fig. 8. f vs Re for different volume fractions ($\emptyset$) at $T_i = 90\ ^oC$

4.4 Influence of anti-freezing agent on thermal performance

Fig. 9 shows the effect of the coolant (EG) on the heat transfer performance of the radiator. Here,

the thermal performance obtained in pure water (H_2O), mixture of H_2O/EG and mixture of H_2O/EG 4% Vol. Al_2O_3 NPs is compared at Re ranging from 4000 to 8000. As observed in Fig. 9, those base fluids consisting of EG have a better heat transfer enhancement than pure-water, because EG as an additive has a higher specific heat capacity and a lower freezing point, which is quite good for automobile radiators. However, the addition of NPs to the existing base fluid containing an anti-freezing agent has excellent thermal performance when compared to others. At $Re = 8\,000$, in contrast to pure water, the Nu is increased by 55.6% by using a mixture of H_2O/EG in a volumetric proportion of $50:50$, while the further addition of 4% Vol. Al_2O_3 NPs to the mixture of based fluid and EG increases the Nu by exactly 70%.

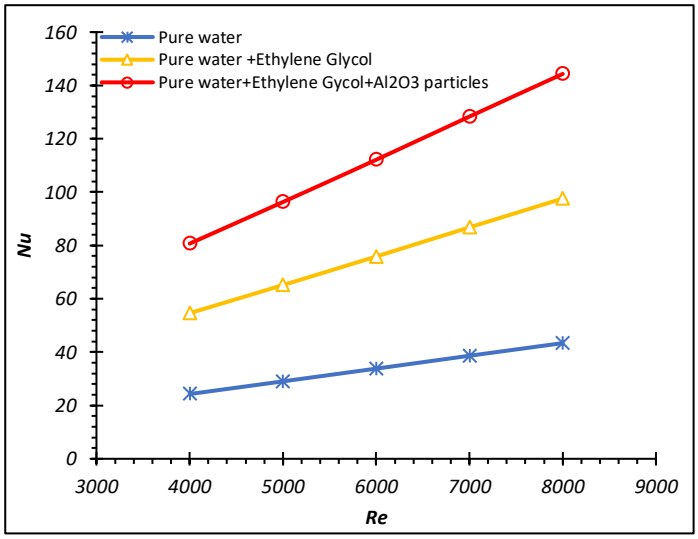

Fig. 9. Nu vs Re for different nanofluids at $T_i = 90\ ^oC$

4.5 Influence of inlet temperature (T_i) on heat transfer rate

Fig. 10 shows the relationship between the heat transfer rate and Re for Al_2O_3/H_2O NAF with a volume fraction of 4% for T_i of $90\ ^oC, 75\ ^oC\ and\ 60\ ^oC$. As shown in the plot, the heat transfer rate slightly rises with Re and T_i. At Re of 8 000, the highest heat transfer rate of 167.94 KW was reported at a 90^oC inlet temperature, followed by $75\ ^oC$ inlet temperature that produced a heat transfer rate of 122.16 KW, and the lowest heat transfer rate of 76.29 KW was observed at a $60\ ^oC$ inlet temperature. Similarly, at $Re = 4\,000$, $90\ ^oC, 75\ ^oC$ and $60\ ^oC$ inlet temperature yield 167.88 KW, 119.92 KW, and 74.98 KW respectively.

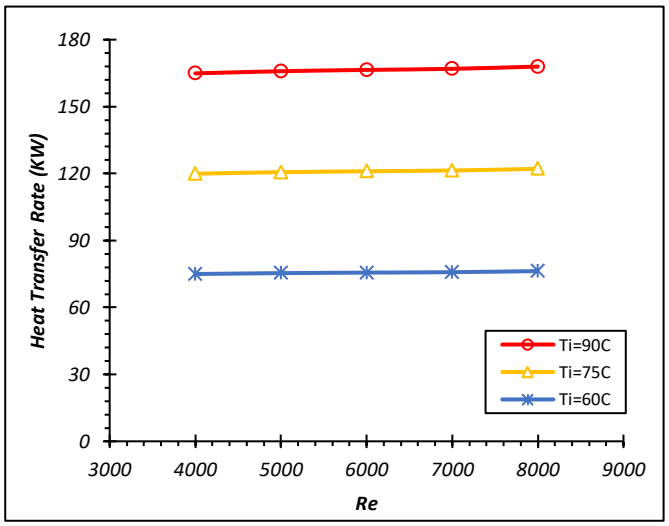

Fig. 10. Heat transfer rate vs Re for different inlet temperatures

4.6 Temperature contour plot

Fig. 11 visualizes the temperature distribution of the automotive radiator. As displayed in Fig.11(a)-11(c), the heated NAF from an automobile's engine block enters the radiator through the inlet at very high temperature, cools as it is being convey through the tubes in the radiator by losing heat to the fins and leave the radiator via the outlet at a low temperature, where it is further utilized to cool the heat generated in the engine. Non-uniform stratified thermal layers are evident on both the fin side and tube side, where the temperature continues to decrease from the top of the radiator to the bottom as heated NAF flows through it.

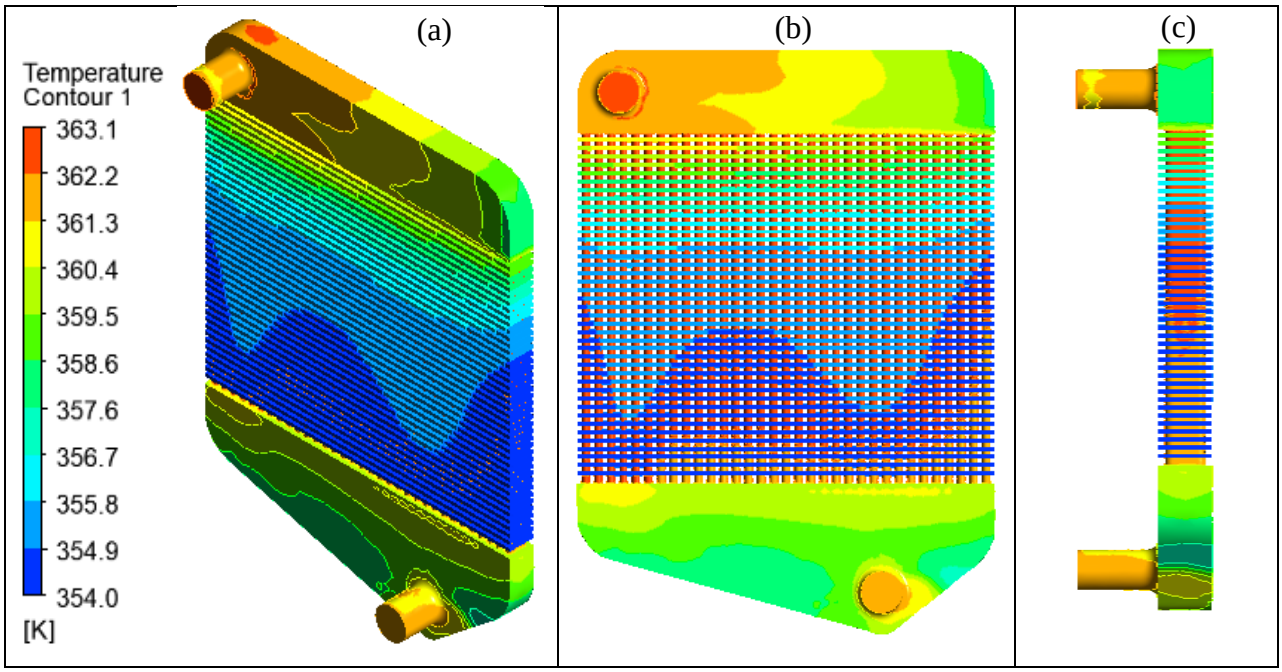

Fig.11. Temperature contour plot for 4% Vol. Al_2O_3 − water nanofluid at Re = 4 000 (a) 3D-view (b) xy- plane at z = 20 mm (c) Side view

4.7 Pressure contour plot

Fig. 12 displays the pressure distribution in the radiator. There is no evidence of pressure drop is visible at the fin side as shown in Fig.12(a). More so, As shown in plot 12(b), the pressure of the NAF decreases as it flows down the radiator, the pressure at the outlet is appreciably lower than that of the inlet.

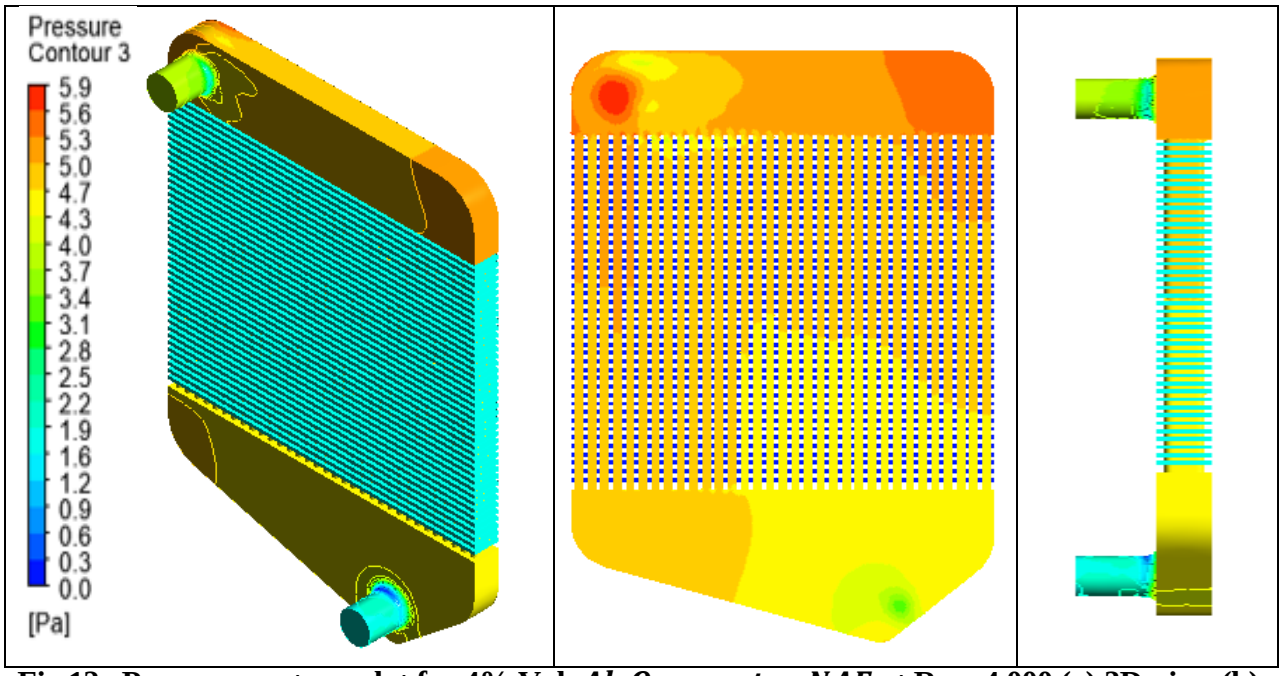

Fig.12. Pressure contour plot for 4% Vol. $Al_2O_3 - water\ NAF$ at Re = 4 000 (a) 3D-view (b) xy- plane at z = 20 mm (c) Side view

5. Conclusion

In this study CFD study was conducted to investigate the thermal characteristics of an automotive radiator using pure water (H_2O), mixture of H_2O/EG and Al_2O_3-H_2O/EG NAF at different Reynolds numbers, volume fractions, and inlet temperatures. The following conclusions are drawn:

1. The addition of NPs of a certain volume fraction to the base fluid enhances the heat transfer rate of the automotive radiator.
2. For all the nanoparticle concentrations considered, the heat transfer rate, Nu, and ΔP all increases as the Reincreases.
3. Among others, an automotive radiator operated with Al_2O_3-H_2O/EG NAF yielded the highest value of Nu and heat transfer rate.
4. At $4\,000 \leq \mathrm{Re} \leq 8\,000$, continuous increase in the volume fraction of Al_2O_3 NPs in the base fluid from 0% to 4% yields no appreciable changes in skin friction factor.
5. Higher heat transfer enhancement could be achieved by adding EG to the existing NAF which contains H_2O as base dluid.
6. The heat transfer rate of the automotive radiator improves as the inlet temperature increases from 60°C to 90°C.

Acknowledgements

The authors appreciate the support from University of Lagos.

References

Abbasian Arani, A. A., & Memarzadeh, A. (2021). Nanofluid multi-morphology effect on dual-fluid sinusoidal-wavy grooved absorber tube parabolic trough solar collector performances enhancement based on experimental data. *International Communications in Heat and Mass Transfer*, *123*, 105201. https://doi.org/10.1016/j.icheatmasstransfer.2021.105201

Belnap, B. J., Van Rij, J. A., & Ligrani, P. M. (2002). A Reynolds analogy for real component surface roughness. *International Journal of Heat and Mass Transfer*, *45*(15), 3089–3099. https://doi.org/10.1016/s0017-9310(02)00042-x

Chavan, D., & Pise, A. (2013). Performance investigation of an automotive car radiator operated with nanofluid as a coolant. *Journal of Thermal Science and Engineering Applications*, *6*(2), 5.

https://doi.org/10.1115/1.4025230

Chon, C. H., Kihm, K. D., Lee, S. P., & Choi, S. U. S. (2005). Empirical correlation finding the role of temperature and particle size for nanofluid (Al2O3) thermal conductivity enhancement. *Applied Physics Letters*, *87*(15), 153107. https://doi.org/10.1063/1.2093936

Eastman, J. A., Choi, S. U. S., Li, S., Yu, W., & Thompson, L. J. (2001). Anomalously increased effective thermal conductivities of ethylene glycol-based nanofluids containing copper nanoparticles. *Applied Physics Letters*, *78*(6), 718–720. https://doi.org/10.1063/1.1341218

Ebrazeh, S., & Sheikholeslami, M. (2020). Applications of nanomaterial for parabolic trough collector. *Powder Technology*, *375*, 472–492. https://doi.org/10.1016/j.powtec.2020.08.005

F.W. Dittus, & L.M.K. Boelter. (1930). Heat transfer in automobile radiators of the tubler type. *Ci.Nii.Ac.Jp*, *2*, 1–18. https://ci.nii.ac.jp/naid/10021874270/

Fedele, L., Colla, L., & Bobbo, S. (2012). Viscosity and thermal conductivity measurements of water-based nanofluids containing titanium oxide nanoparticles. *International Journal of Refrigeration*, *35*(5). https://doi.org/10.1016/j.ijrefrig.2012.03.012

Gadhave, P. and K. P. (2012). Enhancement of Forced Convection Heat Transfer over Dimple Surface. *International Multidisciplinary E-Journal*, *1*(2), 51–57. https://www.shreeprakashan.com

Guntaka, A., Dey, S., Somani, A., Gokhale, M., & Tamma, B. (2009). Cooling Enhancement of Radiators Using Dimples and Delta Winglets. *ASME 2009 Heat Transfer Summer Conference Collocated with the InterPACK09 and 3rd Energy Sustainability Conferences*, 675–683. https://doi.org/10.1115/ht2009-88110

Habeeb, H., Mohan, A., Norani, N., & Azman, M. (2020). Analysis of Engine Radiator Performance at Different Coolant Concentrations and Radiator Materials. *International Journal of Recent Technology and Engineering*, *8*(6), 2277–3878. https://doi.org/10.35940/ijrte.F7866.038620

Heris, S. Z., Shokrgozar, M., Poorpharhang, S., Shanbedi, M., & Noie, S. H. (2014). Experimental Study of Heat Transfer of a Car Radiator with CuO/Ethylene Glycol-Water as a Coolant. *Journal of Dispersion Science and Technology*, *35*(5), 677–684. https://doi.org/10.1080/01932691.2013.805301

Ho, C. J., Chen, M. W., & Li, Z. W. (2008). Numerical simulation of natural convection of nanofluid in a square enclosure: Effects due to uncertainties of viscosity and thermal conductivity. *International Journal of Heat and Mass Transfer*, *51*(17–18), 4506–4516. https://doi.org/10.1016/j.ijheatmasstransfer.2007.12.019

Incropera, F., DeWitt, D., Bergman, T., & Lavine, A. (1996). *Fundamentals of heat and mass transfer* (5th ed.). Wiley. http://www.mid-contracting.com/sites/default/files/webform/careers_webform/_sid_/pdf-fundamentals-of-heat-and-mass-transfer-frank-p-incropera-david-p-dewitt-pdf-download-free-book-7841c05.pdf

Li, P., Zhang, D., & Xie, Y. (2014). Heat transfer and flow analysis of Al2O3-water nanofluids in microchannel with dimple and protrusion. *International Journal of Heat and Mass Transfer*, *73*. https://doi.org/10.1016/j.ijheatmasstransfer.2014.02.042

Manca, O., Nardini, S., Ricci, D., & Tamburrino, S. (2012). Numerical investigation on mixed convection in triangular cross-section ducts with nanofluids. *Advances in Mechanical Engineering*, *2012*. https://doi.org/10.1155/2012/139370

Masoumi, N., Sohrabi, N., & Behzadmehr, A. (2009). A new model for calculating the effective viscosity of nanofluids. *Journal of Physics D: Applied Physics*, *42*(5). https://doi.org/10.1088/0022-3727/42/5/055501

Nabil, T., Elfarran, M., & Farag, A. (2020). Investigation the Cooling Performance of Vehicle Engines Using Radiator with Nano-Fluid as a Coolant. *Journal of Nanofluids*, *9*(3), 187–195. https://doi.org/10.1166/jon.2020.1742

Nguyen, C. T., Roy, G., Gauthier, C., & Galanis, N. (2007). Heat transfer enhancement using Al2O3–water nanofluid for an electronic liquid cooling system. *Applied Thermal Engineering*, *27*(8–9), 1501–1506. https://doi.org/10.1016/j.applthermaleng.2006.09.028

Oliet, C., Oliva, A., Castro, J., & Pérez-Segarra, C. D. (2007). Parametric studies on automotive radiators. *Applied Thermal Engineering*, *27*(11–12), 2033–2043. https://doi.org/10.1016/j.applthermaleng.2006.12.006

Pak, b. C., & cho, y. I. (2007). Hydrodynamic and heat transfer study of dispersed fluids with submicron metallic oxide particles. *Experimental Heat Transfer*, *11*(2), 151–170. https://doi.org/10.1080/08916159808946559

Peyghambarzadeh, S. M., Hashemabadi, S. H., Hoseini, S. M., & Seifi Jamnani, M. (2011). Experimental

study of heat transfer enhancement using water/ethylene glycol based nanofluids as a new coolant for car radiators. *International Communications in Heat and Mass Transfer*, *38*(9), 1283–1290. https://doi.org/10.1016/j.icheatmasstransfer.2011.07.001

Peyghambarzadeh, S. M., Hashemabadi, S. H., Jamnani, M. S., & Hoseini, S. M. (2011). Improving the cooling performance of automobile radiator with Al2O3/water nanofluid. *Applied Thermal Engineering*, *31*(10), 1833–1838. https://doi.org/10.1016/j.applthermaleng.2011.02.029

Roy, G., Nguyen, C. T., & Lajoie, P. R. (2004). Numerical investigation of laminar flow and heat transfer in a radial flow cooling system with the use of nanofluids. *Superlattices and Microstructures*, *35*(3–6), 497–511. https://doi.org/10.1016/j.spmi.2003.09.011

Saysroy, A., & Eiamsa-ard, S. (2017). Enhancing convective heat transfer in laminar and turbulent flow regions using multi-channel twisted tape inserts. *International Journal of Thermal Sciences*, *121*, 55–74. https://doi.org/10.1016/j.ijthermalsci.2017.07.002

Ting, K., Mozumder, A. K., & Das, P. K. (2019). Effect of surface roughness on heat transfer and entropy generation of mixed convection in nanofluid. *Physics of Fluids*, *31*(9). https://doi.org/10.1063/1.5111104

Trivedi, P., & and, N. V. (2012). Effect of variation in pitch of tube on heat transfer rate in automobile radiator by CFD analysis. *International Journal of Engineering and Advanced Technology*, *1*(6), 2449–8958. http://citeseerx.ist.psu.edu/viewdoc/download?doi=10.1.1.676.465&rep=rep1&type=pdf

Umirov, N., & Abdurokhmonov, S. (2021). Algorithm for calculating finned plate radiators for the cooling system of automobile and tractor engines. *IOP Conference Series: Earth and Environmental Science*, *868*(1). https://doi.org/10.1088/1755-1315/868/1/012002

Zaharil, H. A. (2021). An investigation on the usage of different supercritical fluids in parabolic trough solar collector. *Renewable Energy*, *168*, 676–691. https://doi.org/10.1016/j.renene.2020.12.090